Proposed Wildfire and Flood Fragility Curves for Transmission and Substation Assets

Capstone Project in Collaboration with Southern California Edison

University of Michigan, SEAS

Charlie Lenk, Xingning SA

Advisor: Michael Craig

April 2026

Table of Contents

1. Introduction 4
   1.1 Relevant Overview of Fragility Curves 4
   1.2 Specific Assets & Hazards of Interest 5
   1.3 Key Deliverables 5
   1.4 Scope of Project Work 6
2. Literature Synthesis 6
   2.1 Fragility Curve Methodology Overview 6
   2.2 State of Fragility Curve Development by Hazard Type 7
   2.3 Wind Fragility Curves as a Methodological Reference 8
   2.4 Wildfire Hazard: Failure Mechanisms and Relevant Models 9
   2.5 Flooding Hazard: Failure Mechanisms and Relevant Models 9
   2.6 Summary and Implications for This Report 10
3. Fragility Curve Development and Interpretation 10
   3.1 Wildfire x Transmission Line Air-Gap Flashover 10
      3.1.1 Planning Question Addressed 10
      3.1.2 Physical Mechanism 10
      3.1.3 Model Formulation 11
      3.1.4 Parameter Assumptions and Interpretation Limits 13
      3.1.5 Resulting Fragility Surface Behavior 13
      3.1.6 Planning-Level Threshold Interpretation 16
      3.1.7 Data That Would Improve the Model 17
      3.1.8 Model Context and Relationship to Source Literature 18
   3.2 Flooding x Substation Equipment 18
      3.2.1 Planning Question Addressed 18
      3.2.2 Physical Mechanism 18
      3.2.3 Model Formulation 19
      3.2.4 Parameter Assumptions and Interpretation Limits 20
      3.2.5 Resulting Fragility Surface Behavior 20
      3.2.6 Planning-Level Threshold Interpretation 21
      3.2.7 Data That Would Improve the Model 22
   3.3 Wildfire x Overhead Conductor Thermal Damage 22
      3.3.1 Planning Question Addressed 22

3.3.2 Physical Mechanism 22
3.3.3 Model Formulation 23
3.3.4 Parameter Assumptions and Interpretation Limits 26
3.3.5 Model Fit and Climate Conditioning Interpretation 26
3.3.6 Planning-Level Threshold Interpretation 29
3.3.7 Data That Would Improve the Model 33
4. Cross-Model Planning Interpretation Summary 33
5. Guidance Memo: Applying Fragility Curves in Utility Planning 33
5.1 Purpose of the Fragility Relationships and Interpretation Limits 33
5.2 Appropriate Decision Contexts 34
5.3 Recommended Calibration Pathways 34
5.4 Suggested Internal Data Priorities 35
6. Translating Fragility Curve Outputs to Transmission Planning Inputs 37
7. References 38

1. Introduction

The reliable delivery of electricity is foundational to the health, safety, and economic well-being of the communities that electric utilities serve. For Southern California Edison (SCE), which operates across approximately 50,000 square miles and provides power to roughly 15 million customers [20], this responsibility is increasingly complicated by the effects of climate change. Rising temperatures, extended drought periods, and shifting precipitation patterns are intensifying the frequency and severity of extreme weather events throughout California [20], placing growing physical stress on the transmission and distribution infrastructure that supports everyday life. SCE's 2022 Climate Adaptation Vulnerability Assessment (CAVA) identified wildfire and flooding as two of the top asset-level vulnerabilities in its service territory: 23% of transmission circuits are sensitive to projected wildfire exposure, and FEMA mapping shows that 23% of their transmission substations are vulnerable to 100-year flood inundation or sea level rise [20]. The CAVA also acknowledged that it "did not quantify potential flood plain changes," a limitation that also motivates the flooding fragility work in this report. As these trends continue, the ability of utilities to anticipate and quantify how individual assets respond to climate-driven hazards is becoming more of a crucial element of sound planning practice.

1.1 Relevant Overview of Fragility Curves

Fragility curves provide a quantitative framework for characterizing the relationship between the intensity of a given hazard and the probability that an asset will reach or exceed a defined damage or failure state. Originally developed within earthquake engineering, fragility curves are now widely applied to hazards including wind, flooding, and wildfire affecting power system infrastructure [1]. Their outputs translate physical exposure into probabilistic terms, enabling planners to model how changes in hazard intensity correspond to changes in expected asset performance. In practice these curves can inform probabilistic outage modeling assumptions, infrastructure investment prioritization, and climate sensitivity analyses that are increasingly required under evolving federal and regional reliability standards [19]. SCE's CAVA concluded that "the industry has not yet defined these design criteria beyond the regular N-1-type contingency or loss-of-load expectation (LOLE) analysis" and that "these current approaches may be insufficient to justify investment at the levels that may be needed" [20], a gap that probabilistic fragility curves are positioned to help close.

Fragility curves have not been uniformly developed across all hazard types. Wind fragility curves for power infrastructure are comparatively well-established, supported by decades of empirical data and structural analysis. Analogous curves for wildfire and flooding, which are two highly relevant hazards to SCE's service territory, remain sparse in the published literature. A review of recent studies confirms that wildfire and flooding represent some of the least developed categories of fragility curve research for power systems [1], [10]. This gap poses an opportunity for improvement, as without defensible probabilistic relationships for these hazard types, utilities are left relying on deterministic thresholds or engineering judgment alone, limiting their ability to incorporate climate risk into planning processes in a rigorous and repeatable way. This report works to address this gap directly. The decision to focus on wildfire and flooding, rather than a more well-researched hazard such as wind, was in part because that is where the team determined that structured and documented guidance is most needed.

1.2 Specific Assets & Hazards of Interest

This report focuses on two main asset-hazard pairs: transmission infrastructure exposed to wildfire conditions, and substation equipment exposed to flooding. These pairs reflect both the geographic concerns of SCE's operational area and hazard categories where fragility curve development is most limited. An important distinction shapes how the wildfire work is scoped. For assets in the direct path of a fire front, damage outcomes are largely deterministic, and the largest planning-relevant question is often related to restoration logistics rather than failure probability. The more probabilistic relationship, and the one the capstone team has found directly useful for planning, is between wildfire-adjacent stressor conditions and the probability of asset failure. Elevated ambient temperatures can also accelerate thermal degradation pathways under sustained loading and heat exposure [11], [12], [13]. These are graded, intensity-dependent effects that vary across the landscape well outside any active fire boundary, and they can influence the spatial risk conditions utilities like SCE evaluate when calibrating Public Safety Power Shutoffs (PSPS).

For flooding, inundation depth relative to equipment elevation serves as the primary intensity measure, and a depth-based, empirically informed screening approach provides the most defensible available structure for this pair. Depth is directly measurable, is identified in the literature as a key flood-vulnerability variable for substations [14], and aligns with the depth, equipment-height, and functionality-based workflow used in Hazus utility-system analyses [23, pp. 70-75]. Covering both these hazard types is in part done because the wildfire work demonstrates an analytical, physics-based approach to fragility curve construction, while the flood work demonstrates a custom, provisional screening model informed by empirical literature and Hazus methodology. Investigating these differing methodologies helped the capstone team develop the guidance memo (section 5), which is organized around helping SCE select an appropriate curve type based on the nature of the hazard, the available evidence base, and available data. Both pairs also map to planning inputs currently treated as static deterministic values independent of climate scenario in transmission planning processes, a gap identified in the companion report analysis of regulatory frameworks and climate data integration [3], [19].

1.3 Key Deliverables

This report delivers three primary outputs:

1. The first is a synthesis of the relevant literature on fragility curve methodologies and the specific asset/hazard relationships studied here, with attention to the strengths and limitations of judgmental, empirical, analytical, and hybrid curve construction approaches (section 2).
2. The second is a set of fragility curves for three models (section 3):
    a. Flashover fragility model for the wildfire/transmission line pair
    b. Flood fragility model for the flooding/substation pair
    c. Thermal damage fragility model for the wildfire/conductor pair

3. The third is a guidance memo describing when and how to apply fragility curves in utility planning contexts, organized as a decision framework covering model selection, probabilistic versus deterministic use, and the utility and publicly available data most relevant for future calibration and improvement (section 5).

This report develops three provisional fragility relationships intended for planning-level screening applications. Each model is presented together with its assumptions, parameter sources, interpretation limits, and potential pathways for improvement.

1.4 Scope of Project Work

In general, this report is oriented toward providing SCE with synthesis, examples, and recommendations regarding fragility curves for climate adaptation and infrastructure planning that are built on credible literature and data outside of the internal work that SCE completes. The hope is that research into this area done from the 'outside-in' can produce interesting insights that can supplement or assist work done internally at SCE. The primary goal was not to produce final, statistically validated fragility curves, but instead to provide SCE with logical and defensible relationships for each pair investigated that could be built on or referenced in the future, while acknowledging the limitations and assumptions these curves have. The fragility curve models developed here use conditional relationships that take hazard intensity as input; they do not currently incorporate projected changes in hazard frequency or intensity over time. These proposed curves should be treated as provisional and not yet up to the standards for use, however a recommended pathway is provided for refining those curves using SCE's internal asset performance data, so that subsequent models could be used in planning. The intent is for the work presented here to serve both as a usable planning resource in the near term and as a structured foundation for more data-intensive curve development over time.

2. Literature Synthesis

2.1 Fragility Curve Methodology Overview

Serrano-Fontova et al. [1] identify four primary methodological approaches for constructing fragility curves, each suited to different conditions of data availability and analytical resources. Understanding these categories is essential for evaluating the suitability of existing models and for selecting an appropriate construction method for a given asset/hazard pair.

Judgmental fragility curves are derived from structured expert opinion and professional judgment. They do not require historical failure data or detailed structural models, making them applicable when observational records are sparse or an asset type is newly deployed. Their primary limitation is susceptibility to expert bias, and their uncertainty bounds are typically wide and difficult to quantify rigorously. Despite this, judgmental curves often represent the only tractable option for hazard/asset combinations that have not accumulated sufficient event data [1].

Empirical fragility curves are constructed from observed failure and non-failure data collected following real hazard events. When sufficient data exist across a meaningful range of hazard intensities, empirical curves can produce reliable probability estimates grounded in actual asset

behavior. Their weakness lies in dependence on data quality and quantity: sparse events at high hazard intensities, inconsistent failure reporting practices, and geographic confounders all introduce uncertainty into the fitted relationships. For hazards with extensive historical records, such as high winds and earthquakes in densely documented regions, empirical methods have produced some of the most widely used curves in the power systems literature [1],[3].

Analytical fragility curves are derived from physics-based or structural models. A representative model of the asset is subjected to simulated hazard loads across a range of intensities, and failure probabilities are computed from the resulting demand-capacity distributions. Analytical methods are particularly valuable when historical failure data are scarce, but the main failure mechanism is physically well-understood, as is the case for transmission line insulation behavior under smoke loading and conductor thermal damage under elevated wildfire exposure. They require careful attention to model assumptions and material variability, which should be explicitly incorporated into the uncertainty characterization [1].

Hybrid fragility curves combine empirical and analytical elements, typically using simulation outputs to supplement sparse observational data or to extrapolate probability estimates beyond observed intensity ranges. Machine learning approaches trained on simulated failure data fall within this category. Hybrid methods are increasingly common in the recent literature and are well-suited to asset/hazard pairs where some operational data exist, but the full intensity range has not been adequately sampled by historical events [1].

A critical decision in any fragility curve construction process is the choice of intensity measure (IM); this is the scalar quantity placed on the x-axis to represent hazard severity. The IM should be physically meaningful, well-correlated with the specific failure mechanism, and measurable or forecastable for planning use. For wind, peak gust speed or 3-second gust speed is standard across literature. For flooding, inundation depth at equipment elevation is the most widely used measure. For wildfire, the choice is less settled as conductor temperature, smoke & ash particle density, and fire exposure variables such as flame length can each serve as primary IMs depending on the failure mechanism [1], [2].

2.2 State of Fragility Curve Development by Hazard Type

The maturity of fragility curve research varies substantially by hazard type. Wind is the most developed category for power system assets, with parameterized curves available for both transmission towers and distribution wood poles across multiple asset classes and age cohorts [5], [6], [7], [8]. These curves have been validated against observed storm damage in multiple countries and are well-integrated into probabilistic resilience assessment frameworks. Their functional form is typically a lognormal cumulative distribution function (CDF), and parameter tables for standard pole and tower classes are available in literature, enabling application without site-specific testing.

Seismic fragility curves for substations are also relatively mature, particularly for high-voltage equipment such as bushings, disconnect switches, and power transformers, drawing on extensive post-earthquake damage surveys across Japan, the United States, and elsewhere [10].

Flooding and wildfire fragility curves for power system assets are among the least developed categories in the current literature [1],[10]. Karagiannakis et al. [10], in their review of fragility models for power grid infrastructure, identified flooding and wildfire as explicit research priorities, noting that parameterized, peer-reviewed curves for these hazard types are sparse or entirely absent for most key asset classes.

2.3 Wind Fragility Curves as a Methodological Reference

Although wind is not a primary subject of this report, the wind fragility curve literature provides the most complete methodological template available for power system assets. It is reviewed here to establish what a well-parameterized fragility curve output looks like in practice, and to introduce the functional forms and parameter structures that inform the wildfire and flood work in later sections.

Structural wind fragility, meaning the probability that a pole or tower fails given a specified wind speed, is well-documented: decades of post-storm damage surveys have produced parameterized lognormal curves for both distribution wood poles and transmission towers across multiple asset classes and age cohorts [6], [7]. Climate-model wind prediction uncertainty is a separate issue: coarse spatial resolution in regional climate projections limits confidence in future extreme wind speed estimates at the corridor scale, making it difficult to translate fragility curves into long-run climate risk assessments [21]. Prediction accuracy and data uncertainty become particularly important considerations when developing longer-term risk assessments and choosing where to allocate time and resources related to planning.

For distribution-level wood poles, multi-dimensional fragility functions express failure probability as a function of wind speed, pole class, height, and age [6]. These functions adopt the lognormal cumulative distribution function form (CDF), which is the most common functional form across the power systems fragility literature [3]:

$$P(DS \geq ds|IM) = \Phi\left[\frac{\ln IM - \mu}{\sigma}\right]$$

In this expression, $P(DS \geq ds|IM)$ represents the probability of a damage state of an asset being reached or exceeded given the intensity measure of the hazard being investigated. Φ is the standard normal CDF, μ is the natural logarithm of the median failure intensity, and σ captures combined uncertainty from material variability and load modeling. A smaller σ produces a steep S-curve with a sharp failure transition, while a larger σ produces a shallower curve indicating greater uncertainty in the failure threshold. For the fragility curves in this report, σ values of 0.35-0.45 for flooding and 0.04 for the wildfire flashover dispersion coefficient reflect moderate-to-low uncertainty in the current parameterized boundaries.

For transmission-level assets, common empirical wind fragility approaches link observed fault rates per unit line length to wind speed bins derived from weather station records, enabling probabilistic failure rate estimation for real network topologies with altitude and terrain exposure corrections [5], [8]. System-level resilience assessment frameworks combine component fragility curves with corridor-level outage aggregation models and parameterized time-to-repair functions, showing an example of how asset-level vulnerability can be transferred into broader

network-level reliability metrics such as loss of load expectation and expected energy not supplied [3], [4].

2.4 Wildfire Hazard: Failure Mechanisms and Relevant Models

Wildfire interacts with power system infrastructure through several physically distinct pathways. Jazebi et al.'s review of wildfire management techniques for the power sector [9] identifies combustion of poles and crossarms, conductor thermal expansion & tensile strength loss due to radiant heating, direct thermal stress on conductor insulation, and vegetation contact as the principal direct-contact failure mechanisms. For assets physically within the fire perimeter, these mechanisms produce outcomes that are largely deterministic: severe damage is the expected result when fire fully reaches an asset location.

The analysis found in this wildfire literature review to be most relevant for planning focuses on wildfire-adjacent stressor conditions and their relationship to asset failure probability. Two mechanisms found to be particularly relevant are discussed below. The first involves smoke and ash particle deposition along transmission line corridors. Smoke particles reduce the dielectric strength of the air gaps that provide electrical insulation between conductors and between conductors and ground, lowering the breakdown voltage and therefore increasing flashover probability in a continuous, intensity-dependent manner [2]. The second involves wildfire heat exposure, which can raise conductor temperature sufficiently to produce elevated aging stress and other thermal damage concerns. Both mechanisms produce graded, probabilistic outcomes that vary with hazard intensity and extend geographically beyond the active fire boundary.

Dian et al. [2] developed a directly applicable quantitative model for the transmission line/wildfire flashover asset/hazard pair. Their work includes an integrated spatial-temporal Cellular Automata Model to predict the spreading of wildfire from ignition points, whose outputs, including predicted temperature and smoke density, directly feed into a more granular line outage model (LOM). This LOM was of specific interest; it estimates the breakdown probability of a transmission line air gap as a function of conductor temperature and smoke + ash particle density, yielding a two-dimensional probability surface rather than a single curve. From this, one-dimensional fragility curve slices can be extracted from this surface by conditioning on a fixed value of one variable, allowing the model to be applied in scenario-specific planning contexts where one stressor quantity is treated as a known input. The group identified that this LOM structure has the potential to be used in many different scenarios and contexts to produce meaningful predictive insights, and related adaptation considerations are addressed in Section 3.

2.5 Flooding Hazard: Failure Mechanisms and Relevant Models

Flooding poses distinct failure risks to electrical substations and associated equipment. Published literature indicates that substations are vulnerable to inundation because floodwater can affect ground-level equipment, while vulnerability is influenced by inundation depth, debris and sediment loading, and the installation height of electrical equipment [14]. These considerations make inundation depth relative to equipment elevation an appropriate intensity measure for planning-level flood fragility work [14]; [23, pp. 71-75].

Depth is a useful intensity measure for this hazard because it is consistent with the substation flood-vulnerability variables emphasized in [14] and with the depth, equipment-height, and functionality-based structure used in Hazus utility-system analyses [23, pp. 70-75]. It is also compatible with user-defined flood depth grids and hydrologic or hydraulic model outputs used in Hazus-based flood analysis [23, p. 19; pp. 71-75].

Hazus provides a useful methodological reference for site-specific flood depth, equipment height, and functional depth in utility-system analysis [23, pp. 70-75], but the substation fragility relationship developed in this report is a custom provisional screening model rather than a directly adopted Hazus substation damage function [23, pp. 70-72]. As a result, site-specific equipment elevations remain an important factor governing how the model should be interpreted and refined [14], [23, pp. 74-75].

2.6 Summary and Implications for This Report

The wind fragility literature provides the functional forms and parameter structures that serve as methodological benchmarks for both the analytical wildfire work and the custom, empirically informed flood screening work. The recurring identification of wildfire and flooding as underdeveloped fragility categories in systematic reviews [1], [10] supports the use of provisional curves that are explicit about their assumptions and their data needs. The wildfire outage modeling literature [2], the wildfire heat-transfer literature [15], [16], [17], [18], and the depth-damage substation literature [14], [23] together provide sufficient grounding for planning-level relationships that, while limited in several ways, still provide key insights that can hopefully help inform SCE's integration of related fragility curves and power system infrastructure adaptation .

The following section presents three provisional fragility models developed using the methodological approaches highlighted in the literature cited in the paragraph above.

3. Fragility Curve Development and Interpretation

This section presents three provisional fragility curve models developed for planning-level screening applications. Each subsection states the planning question, summarizes the physical mechanism, presents the model form & parameter information, and then interprets the resulting probability behavior and refinement needs.

3.1 Wildfire x Transmission Line Air-Gap Flashover

3.1.1 Planning Question Addressed

Probability of transmission-level air-gap flashover under wildfire-adjacent smoke and temperature conditions.

3.1.2 Physical Mechanism

The hazard-asset pair addressed in the first fragility curve is wildfire acting on high-voltage transmission line air-gap insulation. The asset is the insulation path of a high-voltage overhead

transmission line, specifically the air gap between the energized conductor and grounded tower structure or cross-arm, which is the primary dielectric barrier in an air-insulated line.

Smoke particle density in and around the conductor air gap and elevated conductor-zone temperature act together to degrade dielectric strength. Smoke and ash deposition contaminates the insulation path, while higher temperature reduces air density and lowers breakdown voltage. Flashover therefore acts as an abrupt but probabilistic event, and a two-variable treatment is appropriate because dense smoke can occur at moderate temperatures while severe heat exposure can develop under different smoke conditions [2].

3.1.3 Model Formulation

Two intensity measures are used jointly: conductor temperature T (deg C) and normalized smoke density S_{norm} (dimensionless). Conductor temperature is defined as the bulk air temperature in the conductor gap zone and ranges from ambient conditions of about 20 deg C to a 200 deg C ceiling representing the extreme near-flame zone modeled here. Smoke density is represented as a normalized quantity ranging from 0 to 1.0, following [2]'s treatment of smoke density as a fraction of maximum particulate loading (S = 0 when no smoke is present; S = 1.0 when the air gap is fully filled with combustion particulate [2], Eq. 8).

Practically, S_{norm} represents the fraction of maximum particulate loading in the conductor air gap. A value of 0 corresponds to clean air with no smoke present. A value of 1.0 represents the densest smoke conditions observed adjacent to an active crown fire, conditions under which the air gap is effectively saturated with combustion particulate. Intermediate values reflect proportional smoke exposure: S_{norm} = 0.33, an intermediate reference value used later in the threshold discussion, corresponds roughly to conditions several hundred meters downwind of an active fire front, or closer proximity to a lower-intensity surface fire. Mapping real-world smoke observations to this 0-1 scale requires calibration data; satellite aerosol optical depth products or ground-level particulate measurements matched to wildfire outage records are two valid methods identified for future calibration.

The core model computes a modified breakdown voltage U_{op} for the contaminated air gap, then evaluates the probability that the operating voltage U_{op} exceeds this modified threshold.

Eq. 1. $C_s = \frac{1}{9S_{norm}+1}$

The coefficient 9 is set so that at maximum smoke loading (S_{norm} = 1.0), C_s= 1/(9+1) = 0.10, consistent with observations that dense combustion particulate can reduce breakdown voltage to approximately 10% of the clean-air value [2].

Eq. 2. $C_t = clip\left(1 - 0.45\left(\frac{T-20}{200}\right), 0.55, 1.0\right)$

This linear form approximates the temperature correction in [2] (Eqs. 6-7), which uses C_t = delta^m where delta = (273+T_0)/(273+T). The linear approximation closely tracks [2]'s formulation over the 20-200 deg C range; the 0.55 floor corresponds to the correction value at the 200 deg C thermal ceiling.

Eq. 3. $U_{50,clean}(x) = 912.75 \cdot \ln x + 640.8$

Eq. 4. $U_{50,mod} = U_{50,clean} \cdot C_s \cdot C_t$

Eq. 5. $P_{fail} = \Phi\left(\frac{U_{op} - U_{50,mod}}{z \cdot U_{50,mod}}\right)$

Equation 3 reproduces [2]'s reported 500 kV value when x = 14.8 m, which confirms that the logarithm is natural log and gives $U_{50,clean}$ = 3100.3 kV, rounded to 3100 kV here. For the 230 kV case, this report uses x = 1.9 m as a planning proxy within a standard 1.8-2.0 m air-gap range; Eq. 3 then gives $U_{50,clean}$ = 1226.7 kV. U_{op} is set to 600 kV for 500 kV and 260 kV for 230 kV as planning proxies for nominal peak electrical stress. Dian et al. [2] report that z varies from 2% to 8% depending on air gap type and conditions, and use z = 0.04 in their 500 kV case study. This report adopts the same value.

The core model structure, both correction factors, the modified breakdown voltage calculation, and the probabilistic failure formulation, is taken directly from the Line Outage Model (LOM) in Dian et al. [2]. The adaptations made for planning use are: (1) the temperature correction is simplified to a linear form approximating [2]'s expression over the 20-200 deg C range; (2) the model is separated from [2]'s CA fire-tracking system and used as a standalone fragility curve; and (3) parameters are adapted to SCE-relevant voltage classes.

Table 1. Wildfire x transmission flashover model parameters

Parameter	Value	Source	Notes
Conductor temperature T	20-200 deg C	Scenario-conditioning variable for this report	Bulk air temperature in the conductor gap zone.
Normalized smoke density S_{norm}	0-1.0	Directly aligned with [2], Eq. 8 treatment of smoke loading	S_{norm}= 0 is clean air; S_{norm}= 1.0 is the maximum particulate-loading bound used here.
Smoke correction C_s	$\frac{1}{9S_{norm}+1}$	Direct from [2], Eq. 8	Applied without modification.
Temperature correction C_t	$clip\left(1-0.45\left(\frac{T-20}{200}\right), 0.55, 1.0\right)$	Adapted from [2], Eqs. 6-7	Linear approximation of [2]'s delta^m formulation over 20-200 deg C.
Clean-air breakdown voltage $U_{50,clean}$, 500 kV case	3100 kV	Derived from [2], Fig. 3 using x = 14.8 m	Matches the 500 kV case-study air gap in [2].
Clean-air breakdown voltage $U_{50,clean}$, 230 kV case	1226.7 kV	Derived from [2], Fig. 3 using x = 1.9 m planning proxy	1.9 m is used here as a planning proxy for a standard 230 kV air gap.

Operating stress proxy U_{op} , 500 kV case	600 kV	Planning proxy chosen for this report	Planning-level proxy for 500 kV nominal peak stress.
Operating stress proxy U_{op}, 230 kV case	260 kV	Planning proxy chosen for this report	Planning-level proxy for 230 kV nominal peak stress.
Breakdown variation coefficient z	0.04	Parameter choice within [2]'s stated 2%-8% range	Matches the case-study value used in [2].
Modified breakdown voltage $U_{50,mod}$	$U_{50,clean} \cdot C_s \cdot C_t$	Direct from [2], Eq. 9	Computed separately for each voltage class.
Flashover probability P_fail	$\Phi\left(\frac{U_{op} - U_{50,mod}}{z \cdot U_{50,mod}}\right)$	Direct from [2], Eq. 10	Φ denotes the standard normal CDF.

3.1.4 Parameter Assumptions and Interpretation Limits

This model represents a physics-informed screening relationship rather than a statistically calibrated fragility curve. The parameter values are provisional and should be treated as relative risk indices for comparing fire scenarios, not as calibrated values for segment-specific failure prediction. The model structure was developed for high-voltage transmission lines, and adaptation to SCE voltage classes would require replacement of the planning-proxy $U_{50,clean}$ and U_{op} values with values derived from SCE's internal engineering specifications for each voltage class, including actual air gap distances and conductor geometries for the relevant transmission corridors.

3.1.5 Resulting Fragility Surface Behavior

The wildfire flashover fragility surface produces a strong interaction between smoke loading and temperature in both voltage classes, but the transition occurs earlier in the 230 kV parameterization because the operating-stress-to-breakdown ratio is higher. This occurs because $U_{50,clean}$ increases only logarithmically with air-gap length under Eq. 3, while the reduction in operating-stress proxy from 500 to 230 kV is not proportional, leaving the 230 kV case with slightly less dielectric margin under smoke contamination. To make the slice comparison informative, the updated slice plots use voltage-class-specific smoke levels chosen to bracket each case's transition band. For the 500 kV case, the slices at S_{norm} = 0.31, 0.37, and 0.43 produce distinct curves centered near 138 deg C, 92 deg C, and 46 deg C. For the 230 kV case, the slices at S_{norm}= 0.25, 0.31, and 0.38 produce curves centered near 158 deg C, 107 deg C, and 48 deg C. The 230 kV case therefore shifts the failure transition left relative to the 500 kV case while preserving the same two-dimensional model structure.

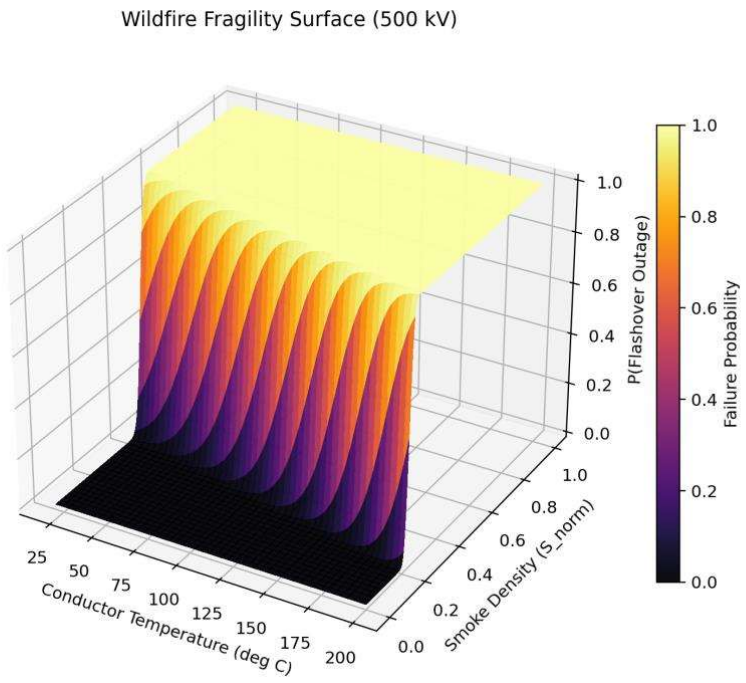


Figure 1. Wildfire fragility surface for the 500 kV case: flashover probability P(outage | T, S_{norm}) as a function of conductor temperature (defined in 3.1.3 as air gap temperature around the conductors in deg C), and normalized smoke density (also defined in 3.1.3).

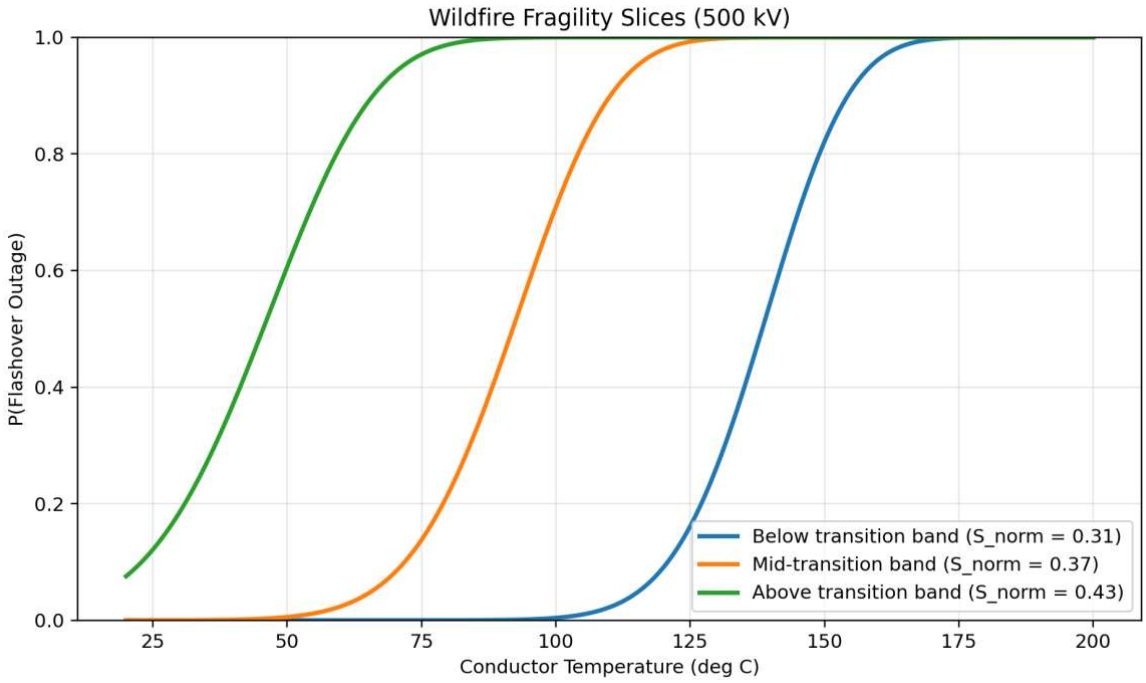


Figure 2. Wildfire fragility slices for the 500 kV case: flashover probability versus conductor temperature at fixed normalized smoke density levels S_{norm}= 0.31, 0.37, and 0.43, selected to bracket the 500 kV transition band.

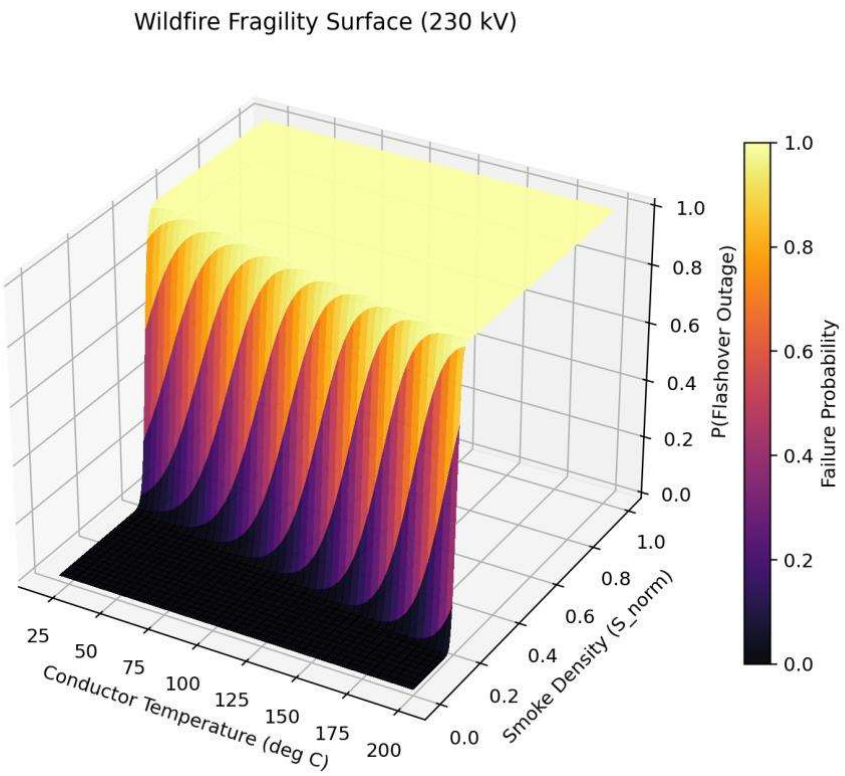


Figure 3. Wildfire fragility surface for the 230 kV case: flashover probability P(outage | T, S_{norm}) as a function of conductor temperature (deg C) and normalized smoke density.

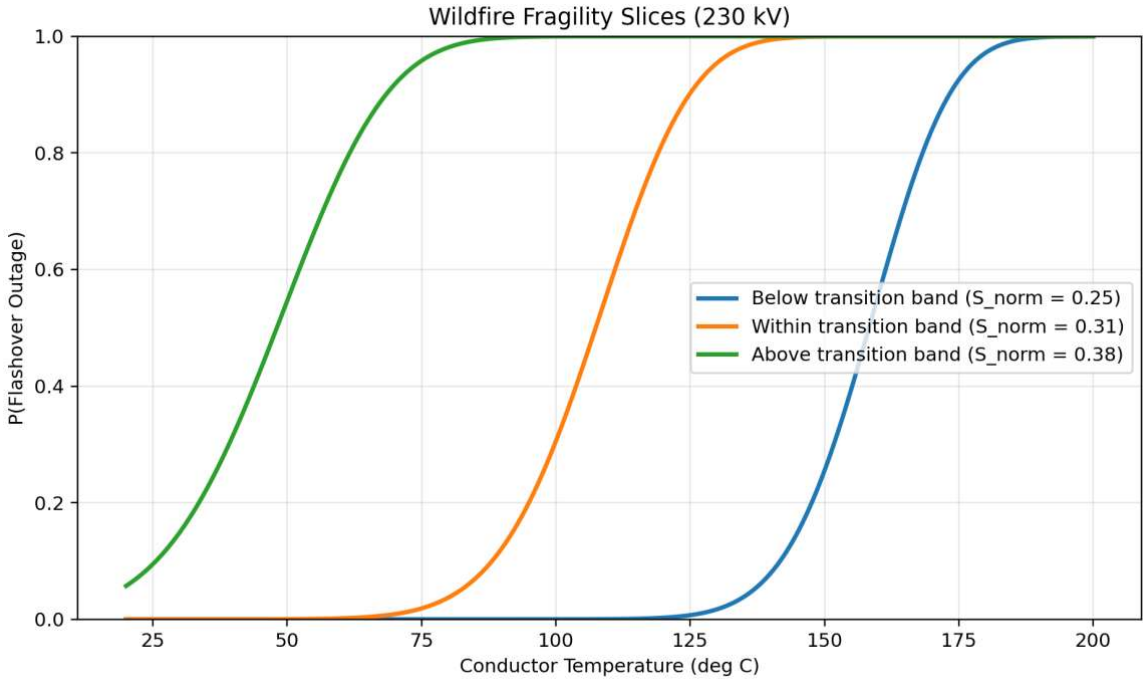


Figure 4. Wildfire fragility slices for the 230 kV case: flashover probability versus conductor temperature at fixed normalized smoke density levels S_{norm}= 0.25, 0.31, and 0.38, selected to bracket the 230 kV transition band.

The 500 kV parameterization is retained as the primary case because it matches the voltage class in [2] and directly corresponds to the Bootleg Fire event described below. The 230 kV case is presented as a secondary parameterization; both cases use the same model structure with voltage-class-appropriate air gap and operating stress values. It is worth noting that the slice values in Figures 2 and 4 are selected for visualization of the transition region in each voltage class; they are not intended as official light-, moderate-, or dense-smoke category boundaries. Relating the relevance of the 500 kV parameterization to California power system infrastructure, during the Bootleg Fire in July 2021, smoke particles from a fire growing to over 240,000 acres in southwest Oregon caused the 500 kV AC Intertie lines to trip repeatedly, reducing them to less than 10% of capacity and the Oregon-California DC path was simultaneously derated 50%. From July 9-13, 2021, California could not access about 5,500 MW of northwest imports, and grid stability was maintained only through an emergency proclamation and customer conservation [20]. This event illustrates a relevant scenario structure for the flashover fragility model: sustained, wide-area smoke exposure at 500 kV scale producing line unavailability without direct fire contact.

3.1.6 Planning-Level Threshold Interpretation

The probability values in Table 2 are computed directly from the flashover model in 3.1.3 at the indicated (T, S_{norm}) points and reflect the 500 kV and 230 kV parameterizations adopted in this report. These are not published thresholds. The region categories and planning interpretations in the right-hand column are a capstone-team overlay: Dian et al. [2] noted that having differentiated responses or criteria based on probability intervals is reasonable but also state that their paper "does not put emphasis on corresponding policymaking" [2]. The framing here maps the model's continuous probability output to the categorical distinctions that FERC 1920-aligned transmission sensitivity studies need. FERC Order No. 1920 (2024) requires transmission providers to incorporate extreme-weather sensitivities into long-term regional transmission planning, including at least one sensitivity scenario per long-term scenario that simulates widespread, sustained outages from extreme events; the companion capstone team report [19] covers the regulatory framework in full.

Table 2. Planning-level threshold regions for wildfire x transmission flashover model parameters

Region	Current parameterization	Planning interpretation
Moderate-smoke temperature band	In the 500 kV case at S_{norm}= 0.33, P_fail = 0.01 at 90 deg C, 0.18 at 110 deg C, and 0.50 at about 123 deg C.	In a FERC 1920 sensitivity study, this is the range where the line should move from baseline availability assumptions to an elevated forced-outage sensitivity rather than an immediate outage case.
Primary 500 kV transition band	At T = 90 deg C, 10%, 50%, and 90% flashover occur at S_{norm}= 0.35, 0.37, and 0.40.	At T = 90 deg C with S_{norm} in this range, flashover probability transitions from roughly 10% to 90%. In a FERC 1920

		sensitivity study, this band represents the shift from 'available with elevated forced outage rate' to 'effectively unavailable for planning purposes.'
High-risk outage band	S_{norm}>= 0.40 with T >= 90 deg C, or S_{norm}= 0.33 with T >= 140 deg C, produces very high flashover probability in the 500 kV case.	These conditions should be modeled as explicit outage scenarios when testing import-constrained, high-load, or wildfire-stress system states.
230 kV comparison band	At T = 90 deg C in the 230 kV case, 10%, 50%, and 90% flashover occur at S_{norm}= 0.31, 0.33, and 0.35.	The 230 kV case reaches planning-relevant unavailability under somewhat lighter smoke, so corridor studies that include both voltage classes should not reuse 500 kV thresholds for 230 kV assets.

The deterministic thresholds in this table are most applicable as scenario-based screening criteria, for example, in a sensitivity study where fire weather conditions are specified as scenario inputs. They are less suited to real-time PSPS trigger decisions, where smoke density at the conductor level is difficult to forecast with sufficient accuracy at the one-to-two-day planning horizon. The model appears to be better suited to pre-season scenario analysis and FERC 1920 sensitivity work as opposed to real-time operational go/no-go decisions. For SCE use, the moderate-smoke and primary 500 kV transition bands are the ones most likely to motivate elevated forced outage rate assumptions for fire-season FERC 1920 sensitivity cases, while the high-risk band is where explicit line-unavailability scenarios could make more sense. The Bootleg Fire event discussed in 3.1.5, during which the 500 kV AC Intertie was reduced to less than 10% of capacity under sustained smoke exposure [20], is a real-world example of conditions that could plausibly fall within the high-risk band.

3.1.7 Data That Would Improve the Model

Three steps were identified that can substantially improve this flashover model:

1. Replace the planning-proxy $U_{50,clean}$ and U_{op} values with values derived from SCE's internal engineering specifications for each voltage class, including actual air gap distances and conductor geometries for the relevant transmission corridors. Referencing the modeling methodology in Dian et al. [2] could help expedite this process.
2. Incorporate conductor height and representative span geometry for more accurate smoke and temperature estimation at the air-gap level
3. Re-embed the fragility function in a fire spread framework, such as a FARSITE-based implementation [16], so tower-by-tower temperature and smoke inputs are generated from corridor-specific fire behavior. Outage logs with wildfire cause codes, PSPS activation records, and corridor-level smoke exposure estimates all could provide valid calibration options.

3.1.8 Model Context and Relationship to Source Literature

The core physics in this subsection come directly from the Line Outage Model (LOM) in Dian et al. [2]. In the source paper, the LOM is embedded within a broader wildfire early warning system that uses a Cellular Automata fire-spread model to generate time-varying smoke and temperature conditions along the transmission corridor and at individual line poles. This report extracts the breakdown-probability component from that larger system and uses it as the basis for a standalone planning-level fragility curve.

The one-dimensional slice representations in Figures 2 and 4 are a planning-oriented adaptation in this report. They are intended for scenario-specific planning questions where one intensity-measure dimension is held fixed and the other is varied to show the flashover transition more clearly. A further planning-oriented extension in this report is the 230 kV parameterization. Dian et al. [2] present the LOM for a 500 kV case study; this report applies the same model structure to a secondary 230 kV case using voltage-class-specific air-gap and operating-stress proxies so the flashover transition can be compared across SCE-relevant transmission classes. Re-embedding the same breakdown model in a spatial fire-tracking framework, using something like FARSITE [16] as the fire-spread model, would restore the dynamic capability in [2] and is a natural next step for operational development.

3.2 Flooding x Substation Equipment

3.2.1 Planning Question Addressed

Probability that substation equipment reaches or exceeds defined flood damage states at a given water height above the reference equipment elevation used in this screening model.

3.2.2 Physical Mechanism

The hazard-asset pair addressed in the second fragility curve is flood inundation acting on substation electrical equipment.

For planning purposes, the asset class is represented as a grouped category including transformers, circuit breakers, disconnect switches, control equipment, and associated cable terminations, consistent with the substation-focused component discussions in [14] and the electric power substation facility category in Hazus [23, pp. 70-72].

Published literature indicates that substations are vulnerable to inundation because floodwater can enter ground-level and low-elevation equipment, while vulnerability is influenced by inundation depth, debris and sediment loading, and the installation height of electrical equipment [14].

For this custom screening model, water height above equipment base elevation is used as the intensity measure because it combines the flood exposure variable emphasized in [14] with the equipment-height and functionality concepts used in Hazus utility-system analyses [23, pp. 70-75].

3.2.3 Model Formulation

The intensity measure is flood inundation depth h above equipment base elevation, measured in meters.

In this report, equipment base elevation is defined as the elevation of the lowest installed vulnerable component represented in the grouped asset class.

Where site-specific survey data are unavailable, the example calculations assume that this reference elevation is approximately 0.0-0.3 m above finished yard grade; this range is a provisional planning assumption and not a directly sourced value from [14] or [23].

This intensity measure is compatible with site-specific flood depth grids and hydrodynamic flood outputs of the type used in Hazus-based facility analyses [23, pp. 70-75].

For screening purposes, each fragility curve is represented by a lognormal cumulative distribution function (CDF):

$$P(DS \geq DS_k | h) = \Phi\left[\frac{\ln h - \ln m_k}{\beta_k}\right]$$

where h is flood inundation depth above equipment base elevation, m_k is the median inundation depth threshold for damage state k, β_k is the log-standard deviation for damage state k, and Φ is the standard normal CDF. This lognormal form is a custom modeling choice for the present report and should not be interpreted as a directly published Hazus fragility function for substations. Four damage states are defined:

- DS1 (Minor): Initial wetting of low-elevation equipment or limited water intrusion affecting peripheral components, with inspection, drying, and minor repair required; short outage duration.
- DS2 (Moderate): Floodwater reaches multiple low-elevation equipment elements or control components, causing repairable damage and limited component replacement; outage from days to about one week.
- DS3 (Extensive): Inundation reaches critical equipment elevations and causes major damage to the grouped asset class, requiring substantial repair or replacement of key components; outage from weeks to months.
- DS4 (Complete): Flooding results in near-total functional loss of the grouped substation equipment representation, requiring major replacement or reconstruction before restoration; outage from months to more than one year.

These DS1-DS4 damage states are planning categories developed for this report, informed by the general flood vulnerability literature [14] and Hazus methodology [23].

Table 3. Flooding x substation model parameters

Parameter	Value	Source Type	Notes
Intensity measure h	Water height above equipment base elevation	literature-derived	Based on inundation depth and equipment-height/functionality concepts in [14] and [23, pp. 70-75]

DS1 median m_k	0.15 m	provisional planning assumption	Initial wetting threshold selected for grouped low-elevation equipment
DS2 median m_k	0.45 m	provisional planning assumption	Moderate-damage screening threshold selected for planning use
DS3 median m_k	0.85 m	provisional planning assumption	Extensive-damage screening threshold selected for planning use
DS4 median m_k	1.35 m	provisional planning assumption	Complete-loss screening threshold selected for planning use
DS1 dispersion β_k	0.45	provisional planning assumption	Selected to represent a relatively gradual onset of minor damage
DS2 dispersion β_k	0.40	provisional planning assumption	Selected for planning-level transition behavior
DS3 dispersion β_k	0.35	provisional planning assumption	Selected for planning-level transition behavior
DS4 dispersion β_k	0.35	provisional planning assumption	Selected for planning-level transition behavior

The median thresholds and dispersions above are provisional project-specific values selected for planning-level screening. They were chosen to represent an ordered increase in damage severity with inundation depth and to produce stable, monotonic fragility curves over the depth range examined; they are not directly calibrated empirical estimates from [14] or [23].

3.2.4 Parameter Assumptions and Interpretation Limits

This model is a custom, provisional screening relationship rather than a facility-specific calibrated fragility curve. The median thresholds were selected so that each damage state corresponds to a progressively more severe level of inundation exposure, and the spacing between thresholds was chosen to avoid unrealistically abrupt overlap among damage states. The dispersions were then chosen to generate smooth, monotonic exceedance curves that produce interpretable screening transitions over the flood-depth range most relevant to planning analysis. These values were informed by the general flood-vulnerability variables emphasized in [14] and the depth, equipment-height, and functionality-based modeling structure described in [23], but they are not directly calibrated empirical estimates from those sources.

3.2.5 Resulting Fragility Surface Behavior

Under the current provisional parameterization, moderate-to-extensive damage risk increases rapidly between 0.5 m and 1.0 m of inundation.

- At 0.3 m depth, P(DS>=2) = 0.16 and P(DS>=3) = 0.002.
- At 0.6 m, P(DS>=2) = 0.76 and P(DS>=3) = 0.16.
- At 1.0 m, P(DS>=2) = 0.98 and P(DS>=3) = 0.68.

This 0.5-1.0 m interval is the steepest transition zone in the current parameterization, so small changes in effective flood depth produce large changes in DS2 and DS3 exceedance probability.

These results are outputs of the custom screening model defined above and should not be interpreted as observed empirical failure frequencies.

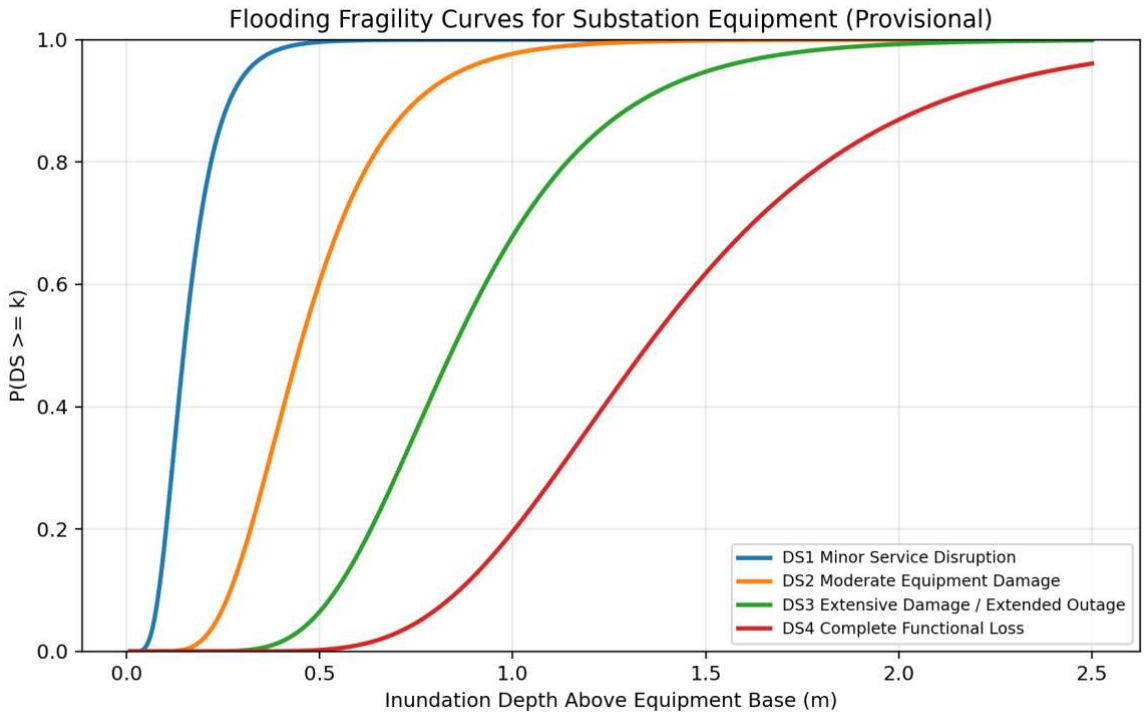


Figure 5. Flooding fragility curves: exceedance probability P(DS >= k | h) for damage states DS1-DS4 as a function of inundation depth above equipment base elevation (meters). Parameters are provisional and are intended just for screening use.

3.2.6 Planning-Level Threshold Interpretation

Thresholds reflect the current parameterization only and should not be interpreted as universal substation failure depths.

Table 4. Planning-level threshold regions for flooding x substation model

Region	Current parameterization	Planning interpretation
Screening concern region	Around 0.3-0.5 m inundation depth, DS2 begins to rise while DS3 remains low	Early review zone for lower-elevation substations and control equipment under the current parameterization.

Elevated probability region	At 0.6 m, P(DS>=2) = 0.76 and P(DS>=3) = 0.16	Main transition band for mitigation screening and flood-barrier evaluation under the current parameterization.
High-risk region	At 1.0 m, P(DS>=2) = 0.98 and P(DS>=3) = 0.68	Current parameterization places this range in a high extensive-damage screening band.
Severe loss region	At 1.5 m, P(DS>=3) = 0.95 and P(DS>=4) = 0.62	Indicates strong potential for extensive damage and a meaningful probability of complete loss in the current screening model.

3.2.7 Data That Would Improve the Model

- Equipment elevation surveys are identified as the highest-impact improvement because both the literature and the Hazus framework indicate that equipment height or elevation strongly influences flood damage and functionality [14]; [23, pp. 70-75].
- Post-event damage documentation from flood-affected substations would support future calibration or Bayesian updating of the median damage-state parameters.
- Site-specific flood hazard mapping would allow the curve to be tied to actual substation exposure distributions and would reduce uncertainty in the current screening assumptions [23, pp. 70-75].

3.3 Wildfire x Overhead Conductor Thermal Damage

3.3.1 Planning Question Addressed

Probability that wildfire heat exposure drives conductor temperature rise above a planning-level thermal damage threshold.

3.3.2 Physical Mechanism

The third fragility model addresses wildfire acting on overhead conductors through a different failure pathway than the flashover model. Instead of electrical breakdown across an air gap, this model evaluates whether wildfire heat exposure raises conductor temperature enough to represent elevated aging stress and thermal damage concern for the conductor itself.

Combined convective and radiative heat transfer from a nearby fire drives this response. Flame spread, flame geometry, wind, conductor height, and related exposure variables affect the incident heat flux, which then determines conductor temperature rise. A probabilistic treatment is required because wildfire exposure variables (flame geometry, wind, and residence time) vary independently and interact nonlinearly in the heat-transfer formulation, preventing a deterministic threshold representation.

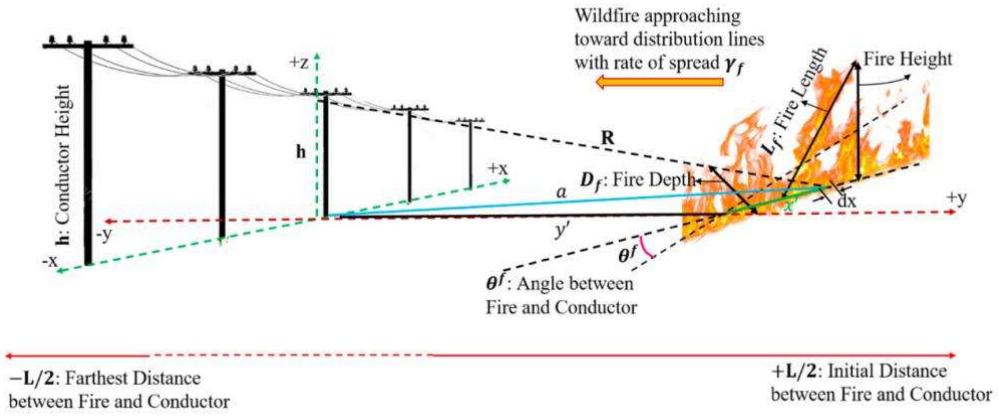


Figure 6. Physical parameters governing wildfire heat transfer to overhead conductors. Reproduced from Nazemi et al. [24], Fig. 1.

3.3.3 Model Formulation

The core wildfire-conductor thermal model and the original parameterized fragility formulation are adapted from Nazemi et al. [24]. This report retains the heat-transfer structure from [24] while using a planning-oriented Monte Carlo implementation rather than the closed-form logistic-regression fragility surface in the source paper.

The failure state is defined as a conductor temperature rise exceeding 25 deg C above baseline conditions, consistent with the binary failure criterion in [24] (Section III-B, Eq. 7). In this report the threshold serves as a screening-level indicator of elevated conductor aging stress rather than an immediate physical failure point.

The model links wildfire conditions to conductor vulnerability through four steps:

(1) wildfire and geometry inputs are sampled across physically admissible ranges
(2) wildfire spread and flame geometry are calculated
(3) combined convective and radiative heat transfer to the conductor is estimated
(4) conductor temperature rise is compared against the threshold.

The core physical relationships, adapted from [24], are as follows:

$$\gamma_f = 0.773 * V_w^{0.707} * \exp(0.062S - 0.039M_s) * FD^{0.188}$$

$$D_f = \gamma_f * \tau$$

$$I_B = 185.2 * L_f^{1.842}$$

$$W_c = 22 * C_f * \left(\frac{D_f}{\gamma_f}\right) * cbrt\left(\frac{I_B^2}{h^5}\right)$$

$$W_r = \frac{I_B * Cos(\theta)}{10 * \gamma_f} * \left[\left(\ln\left(\frac{l}{h}\right) + \ln\left(1 + \left(\sqrt[2]{\left(1 + \left(\frac{h}{l}\right)^2\right)}\right)\right)\right]\right]$$

$$W_T = W_c + W_r$$

$$Faliure = 1\ if\ \Delta_T > 25℃, else\ 0$$

$$FC(x) = \left(\frac{1}{K}\right) * \sum \Delta_{T_{k(x)>25℃}}$$

Failure probability is estimated using a Monte Carlo simulation framework with N = 100,000 samples. The Monte Carlo structure was decided upon because the model contains multiple stochastic inputs, and no closed-form solution for failure probability. It captures exposure variability, represents uncertain wildfire conditions, and produces uncertainty bands rather than deterministic triggers.

Table 5. Wildfire transmission line parameters

Parameter	Value	Source Type	Notes
Temperature-rise threshold	Δ_T> 25 deg C	planning proxy	Screening-level indicator of elevated conductor aging stress
Flame residence time τ	Median 11.6 s, log-scale standard deviation 0.343, truncated to [2 s, 120 s]	literature-informed	Provisional values consistent with documented surface fire residence times [15], [16]
Slope S	-6 to 17 deg	scenario-conditioning variable	Physically admissible wildfire terrain range
Fuel depth FD	0.1-5.5 cm	scenario-conditioning variable	Physically admissible fuel range
Conductor height h	6.1-38.1 m	scenario-conditioning variable	Transmission geometry range
Wind speed V_w	0.5-80.47 km/h	scenario-conditioning variable	Wildfire exposure background variable
Flame length L_f	0.1-4.2 m	scenario-conditioning variable	Primary severity variable in the threshold interpretation
Flame tilt angle theta	0-90 deg	scenario-conditioning variable	Geometric exposure range
Convective coefficient C_f	mean =0.06	literature-informed	Clipped normal assumption used in the heat-transfer model
Ambient temperature range (provisional)	T_min = 46.9 deg F, T_max = 72.7 deg F	literature-derived	Annual mean TMIN and TMAX normals from NOAA 1991–2020 Climate Normals for representative California stations [22]; planning-level estimates only that do not represent distributional extremes

Adaptations were made to the Nazemi et al. [24] source framework for planning use; these are summarized in Table 6.

Table 6. Model upgrade details

Aspect	Nazemi baseline	Capstone adaptation
Core heat-transfer backbone	retained	retained
Failure logic	ΔT > 25°C	retained as planning proxy
Ambient temperature conditioning	not included	added
Fuel moisture conditioning	simpler baseline treatment	conditioned on ambient temperature
Residence time	implicit / baseline treatment	explicit lognormal assumption
Output structure	closed-form parameterized FC	Monte Carlo + CI-based scenario slices
Planning use	general fragility modeling	SCE planning screening

3.3.4 Parameter Assumptions and Interpretation Limits

This model represents a physics-based screening relationship rather than a calibrated asset-specific fragility curve. The heat-transfer backbone and ACSR-95 conductor constants are taken directly from [24]; input ranges are provisional placeholders consistent with [24]'s parameter tables. The capstone-specific adaptations not present in the source framework include: ambient-temperature conditioning from NOAA 1991–2020 Climate Normals [22], a fuel moisture relationship that conditions M_s on ambient temperature, and the specific lognormal residence-time distribution (median 11.6 s, log-scale σ = 0.343). Wind is treated as a scenario-conditioning input rather than a monotonic risk driver because higher wind speeds shorten effective local exposure time through inverse dependence on γ_f.

3.3.5 Model Fit and Climate Conditioning Interpretation

The following figures are used to interpret internal model fit and the joint influence of key climate-conditioning variables on simulated conductor failure behavior.

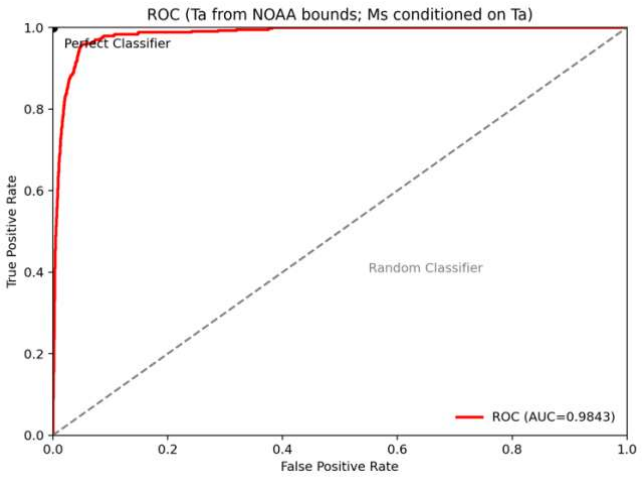


Figure 7. Model ROC accuracy

This figure presents the receiver operating characteristic (ROC) curve for the conditioned wildfire-conductor classifier. The curve remains close to the upper-left corner of the ROC space, with an area under the curve (AUC) of 0.9843, indicating strong discriminatory performance between simulated failure and non-failure cases. It is important to note, however, that this result reflects internal model fit rather than external validation against observed outage records. Specifically, the classifier is evaluated against binary failure labels generated from the thermal damage criterion $\Delta T \geq 25 \circ C$, rather than empirical field observations. Accordingly, the high AUC should be interpreted as evidence that the conditioned classification framework is able to reproduce the simulated failure boundary with high fidelity under the present parameterization. In this sense, the ROC result supports the internal consistency of the Monte Carlo-based screening model and its suitability for subsequent fragility interpretation, while not constituting proof of real-world predictive accuracy.

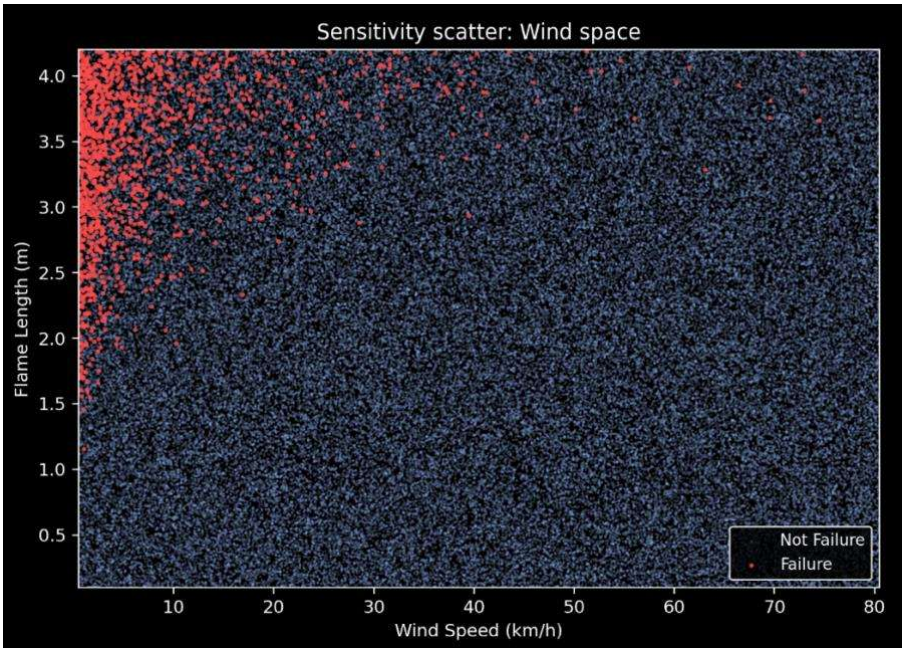


Figure 8. Wind scatter

The upper sensitivity scatter plot illustrates the joint distribution of wind speed and flame length across simulated failure and non-failure cases. Failure points are concentrated more heavily in the region associated with larger flame lengths, indicating that flame length serves as a particularly influential severity variable in the thermal damage pathway. By contrast, wind speed does not produce a simple monotonic failure boundary when viewed in isolation, suggesting that it is better interpreted as a scenario-conditioning variable than as a standalone planning trigger. This pattern is physically consistent with the structure of the heat-transfer model: under lower wind-speed conditions, wildfire spread is slower, increasing the effective local exposure duration and allowing the conductor to absorb more convective and radiative heat. The figure therefore suggests that, although wind contributes materially to the thermal response, its effect is conditional and interaction-based, whereas flame length provides a clearer direct indicator of heightened conductor failure risk.

The lower sensitivity scatter plot shows the relationship between fuel aridity and flame residence time across simulated failure and non-failure realizations. Failure cases are more prevalent under combinations of higher aridity and longer residence time, indicating that drier fuel conditions and more sustained local thermal exposure jointly increase the likelihood that conductor temperature rise will exceed the screening threshold. As in the wind–flame-length plot, the pattern does not imply a sharp one-dimensional threshold; rather, it reveals a probabilistic structure shaped by interacting variables. This result reinforces the rationale for the conditioned Monte Carlo framework used in this study: wildfire-induced conductor vulnerability is not adequately represented by any single input variable alone, but instead emerges from the combined influence of exposure duration, combustion severity, and environmental background conditions. From a planning perspective, fuel aridity and residence time are therefore more

appropriately interpreted as background severity modifiers than as direct deterministic screening criteria.

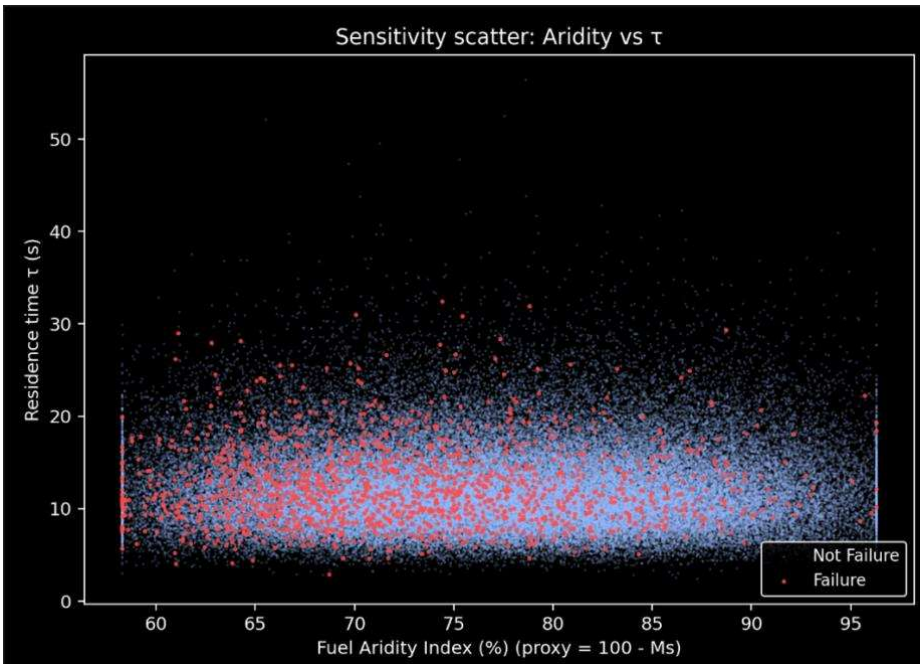


Figure 9 Aridity scatter

3.3.6 Planning-Level Threshold Interpretation

Each CI (conditional index), represent different scenarios. CI-1 to CI-8 are planning-oriented conditional background scenarios defined in this report to slice the multi-dimensional fragility model into interpretable cases.

Table 7. CI level definitions and interpretations

Scenario	Fuel moisture (M_s)	Conductor height (h)	Fuel depth (FD)	Slope (S)	Wind speed (V)	Relative interpretation
CI-1 (hazard)	Low	Low	High	High	Low	Most hazardous background case; combines dry fuel, low clearance, heavy fuel loading, steep slope, and slow spread conditions that prolong local heating
CI-2	Low	Low	Low	High	Low	Hazardous case with dry fuel, low clearance, and steep slope, but lower fuel depth than CI-1
CI-3	Low	High	High	Low	Low	Dry-fuel case with high fuel depth but higher conductor clearance and lower slope
CI-4	High	Low	High	High	Low	Moist-fuel case with low clearance and high fuel loading under steep slope and low wind conditions
CI-5	High	High	High	Low	Low	Higher-clearance case with high fuel depth and low wind background
CI-6	High	High	Low	Low	High	Less hazardous background with moist fuel, high clearance, low fuel depth, low slope, and high wind
CI-7	Low	High	Low	High	High	Mixed background: dry fuel and steep slope, but high clearance, low fuel depth, and high wind
CI-8 (safe)	High	High	Low	Low	High	Safest reference case; combines moist fuel, high clearance, low fuel depth, mild slope, and high wind background

The thermal damage fragility curves show threshold-driven behavior: failure probability remains low across much of the modeled range, then increases rapidly as wildfire exposure becomes

sufficiently intense and sustained. Among all tested variables, flame length and conductor height produce the most stable and actionable thresholds [24].

Flame length is the clearest single severity variable. Across the more hazardous conditional backgrounds, the approximate 50% failure threshold appears at 1.4-2.0 m flame length. Under more moderate backgrounds, the same 50% threshold shifts to roughly 2.8-3.3 m. In the most severe conditional cases, the 90% failure level is reached at approximately 3.8-4.1 m. Conductor height acts as the strongest protective variable. Failure probability declines as clearance increases, with the largest marginal benefit between low-to-moderate heights. Based on current curves, failure probability begins to decline more materially once conductor height exceeds 20-25 m, while heights above 30 m are associated with meaningfully lower risk in most non-extreme cases. The specific threshold values above reflect the conditional Monte Carlo structure used here; the same flame length or conductor height can produce different failure probabilities depending on the background wildfire scenario.

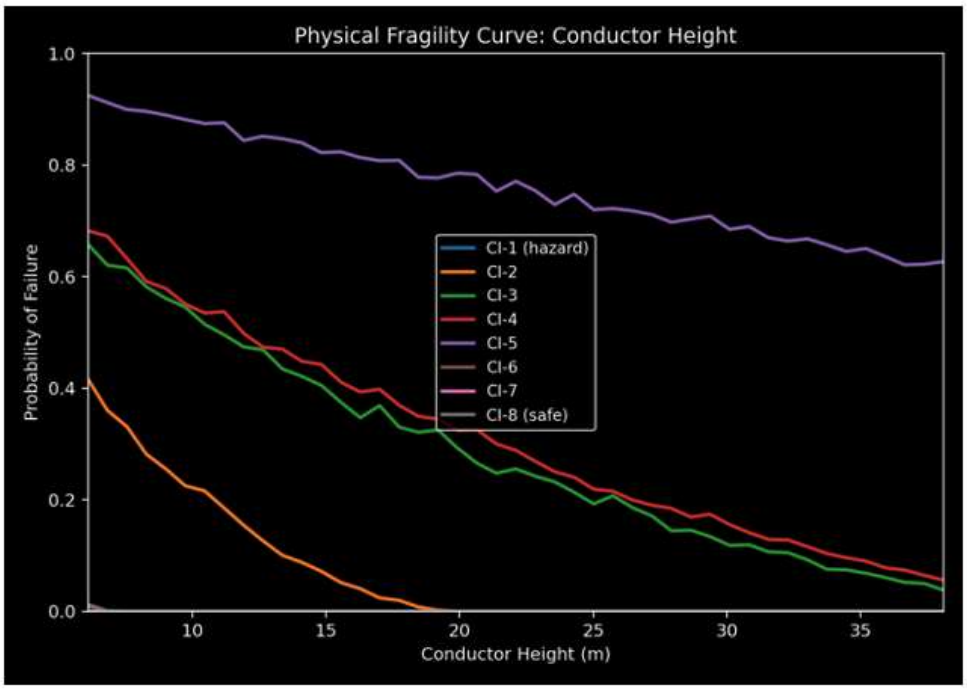


Figure 10. Failure probability as a function of conductor height for conditional background scenarios CI-1 to CI-8, each fixing a different flame length. Generated using the adapted Monte Carlo framework from Nazemi et al. [24].

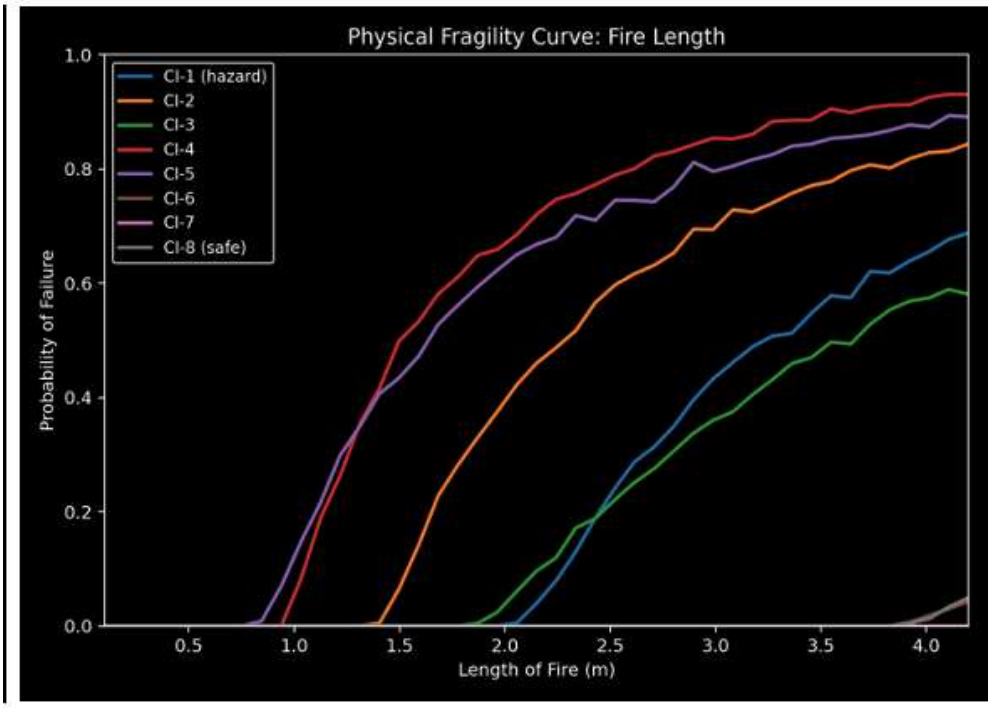


Figure 11. Failure probability as a function of flame length for conditional background scenarios CI-1 to CI-8, each fixing a different wind speed case. Generated using the adapted Monte Carlo framework from Nazemi et al. [24].

Table 8. Description of planning level regions

thresholds reflect current parameterization only

Region	Current parameterization	Planning interpretation
Screening concern region	Flame length of about 1.4-2.0 m produces roughly 50% failure in hazardous conditional backgrounds	Early high-risk transition for exposed conductors in severe wildfire settings
Elevated probability region	Flame length of about 2.8-3.3 m produces roughly 50% failure in more moderate backgrounds	Main screening band for conductor hardening and clearance review
High-risk region	Flame length of about 3.8-4.1 m reaches roughly 90% failure in severe cases	Current parameterization places these cases in the highest thermal-damage screening band
Protective transition region	Conductor height of about 20-25 m marks the main decline in failure probability	Clearance upgrades in this range provide the largest planning benefit
Lower-risk region	Conductor heights above 30 m are associated with meaningfully lower risk in most non-extreme cases	Useful benchmark for identifying spans that already carry stronger thermal clearance margin
Scenario modifiers	Wind speed and fuel aridity do not produce stable standalone thresholds	Use as background severity modifiers, not as direct planning triggers

3.3.7 Data That Would Improve the Model

Conductor height and clearance data from SCE's GIS asset inventory would allow the threshold ranges to be applied to SCE's full inventory of transmission line spans. High Fire Threat District (HFTD) designations matched to conductor configuration data could improve prioritization of where using a model like this would matter most.

4. Cross-Model Planning Interpretation Summary

The three models answer different planning questions and should not be collapsed into a single risk number. The table below provides a side-by-side comparison of the hazard, asset class, output type, and best planning use for each provisional curve.

Table 9. Cross-model planning interpretation Summary

Model	Hazard	Asset Class	Output Type	Best Planning Use
Flashover	Wildfire smoke and heat	Transmission line air-gap insulation	Flashover probability	Operational availability screening and PSPS sensitivity review
Thermal damage	Wildfire heat exposure	Overhead conductors	Thermal damage probability	Clearance review, conductor hardening prioritization, and aging-stress screening
Flood	Inundation	Substation equipment	Damage-state exceedance probability	Capital risk screening and flood mitigation prioritization

The two wildfire models are complementary rather than interchangeable. The flashover model is most useful when the planning question is temporary electrical availability under smoke and heat exposure. The thermal damage model is more useful when the planning question is related to physical conductor vulnerability and the risk-reduction benefit of clearance improvements or line-hardening measures. The flood model translates water height above equipment base elevation into damage-state exceedance and is best suited to site-level flood exposure screening.

5. Guidance Memo: Applying Fragility Curves in Utility Planning

This section aims to provide practical guidance to complement ongoing work by SCE engineers and planners on how to select, apply, and interpret the fragility curves developed in this report. It is organized as a short decision memo rather than a step-by-step procedure, because the right approach depends on the planning question being asked, the data available, and the decision stakes.

5.1 Purpose of the Fragility Relationships and Interpretation Limits

The fragility relationships in this report are planning-level screening tools. They translate hazard intensity into conditional probability of failure or damage-state exceedance, but they do not by

themselves estimate how often those conditions occur under future climate scenarios. For practical use, the main takeaway is not the exact probability number by itself, since that still depends on unvalidated parameter assumptions. What matters more is the overall risk pattern: which conditions push the model into higher-risk territory, which mitigation variables have the strongest influence, and also where better data would most improve confidence.

5.2 Appropriate Decision Contexts

Fragility curves typically produce a continuous probability function, but many planning workflows still require either a probability value at a specific input or a binary pass/fail threshold. The output format should match the decision context.

Table 10. Decision context and recommended fragility curve type examples

Decision Context	Recommended Output Format	Rationale	Example Use
FERC 1920 / WECC sensitivity study	Probabilistic (full curve)	Need outage probability distribution across a scenario range	Apply P_fail(T, S_{norm}) to wildfire-exposed 500 kV and 230 kV transmission corridors under a specified FERC 1920 or WECC sensitivity scenario.
PSPS pre-event screening	Deterministic threshold	Speed matters; probabilistic output adds little value for binary go or no-go decisions	Flag corridors where S_{norm}> 0.38 and T > 90 deg C for pre-event screening; not intended for real-time operational triggering.
Capital investment prioritization	Both: probability for ranking, threshold for triage	Probability enables ranking by expected loss; threshold enables fast filtering	Rank substations by P(DS>=3) at a given flood return period
Clearance design review	Deterministic threshold with probabilistic backup	Engineers need an actionable rule; probability provides context	Identify spans with h < 20 m in HFTD zones and review probabilistic output for 15-25 m
Post-event damage assessment	Deterministic or empirical	Actual exposure is known; probabilistic framing is no longer needed	Compare observed damage state to model-predicted DS exceedance at measured depth

Deterministic thresholds should not be treated as sharp failure boundaries. The normal and lognormal CDF forms used in all three models produce smooth transitions, not step functions. This is especially relevant in the 0.5-1.0 m flood depth range and the 1.5-3.0 m flame length range, where a small change in conditions can produce a large change in failure probability.

5.3 Recommended Calibration Pathways

The four-fragility-curve classification framework follows Serrano-Fontova et al. [1], while the mapping from data availability to recommended modeling approaches and fragility curve

upgrades represent a synthesis developed in this report based on the literature review in Section 2.

Table 11. Recommended fragility curve framework and corresponding recommendations for improvement via calibration & integration

Data Situation	Recommended Method	Output Quality	Upgrade Path
No failure data available but failure mechanism is well understood (e.g. dielectric breakdown or thermal aging)	Analytical	Can be a defensible proxy: parameters will require calibration	Calibrate with outage logs once available
At least some failure data available and a well-validated framework exists, (e.g. HAZUS for substation flooding)	Empirical	Likely reliable for general analysis at a population level but site-specific accuracy would be limited	Bayesian update with post-event surveys
No data available, and failure mechanism is not physically modeled	Judgmental	Wide uncertainty; expert-dependent	Replace or improve with analytical or empirical as data accumulates
Moderate data available with some simulation capability	Hybrid	Strongest option when calibrated; Hybrid approach allows for verification and continual refinement across methods	Expand simulation scope and add machine-learning support if data volume supports it

Across most cases, a primary limiting factor is typically the availability of asset-specific failure and exposure data required for calibration.

5.4 Suggested Internal Data Priorities

All three models in this report are provisional, and their planning values would improve with access to utility-specific and publicly available data. The table below identifies relevant data assets by model and the calibration improvement each would enable.

Model	Priority Data Asset	Likely Data Source	Calibration Improvement
Wildfire Flashover	Outage logs with wildfire cause codes and geographic location	SCE internal	Empirically constrain $U_{50,clean}$ and z by voltage class and replace proxy parameters
Wildfire Flashover	PSPS activation records with smoke and	SCE internal	Validate threshold-crossing behavior against actual operating decisions

	temperature conditions at time of action		
Wildfire Flashover	Satellite-derived smoke concentration products, such as NOAA HMS or NASA MODIS AOD	Publicly available	Provide corridor-level smoke exposure estimates for matching to outage records
Thermal Damage	Conductor height and clearance data from GIS asset inventory	SCE internal	Apply planning thresholds to SCE's full inventory of transmission line segments (individual spans between adjacent towers) to identify those with the highest thermal vulnerability based on conductor height and HFTD zone designation.
Thermal Damage	HFTD zone designations matched to conductor configuration data	SCE internal	Prioritize mitigation review to the highest-risk zone and height combinations
Thermal Damage	NOAA meteorological records for temperature, wind, and humidity	Publicly available	Calibrate ambient temperature and wind speed distributions to SCE service territory conditions
Flooding	Equipment base elevation surveys, including transformer sill heights and control-building floor elevations	SCE internal	Replace nominal base elevation assumptions and shift the curve x-axis to a site-specific reference
Flooding	Post-event damage documentation from flood-affected substations	SCE internal	Update median depth parameters and reduce uncertainty on DS2 and DS3 thresholds
Flooding	FEMA flood hazard maps and NOAA Atlas 14 precipitation frequency data	Publicly available	Overlay substation locations against flood return period maps to help determine site-specific exposure

The most immediately actionable of these is equipment elevation survey work for the flooding model. Site-specific equipment elevation data, including transformer pad elevations and other low-elevation vulnerable components, can shift the effective depth at which damage states are triggered without requiring any change to the model structure. For the wildfire models, PSPS activation records combined with matched meteorological data represent the most tractable near-term calibration dataset because the operational records already exist and the main need is corridor-level exposure matching.

The fragility relationships in this report are conditional on hazard intensity inputs and do not yet provide actionable projections of how often those conditions will occur under future climate scenarios. Translating these curves into climate-aware risk estimates requires pairing with forward-looking hazard projections, for example, projected changes in flood return periods from climate models, or changes in fire weather frequency from regional climate assessments.

6. Translating Fragility Curve Outputs to Transmission Planning Inputs

Current transmission planning relies on static reliability assumptions not designed to account for climate hazard intensity or asset-level failure mechanisms. The companion report completed for this capstone project addresses the planning process side, documenting where current California transmission planning frameworks fall short of incorporating climate-driven asset-level failure data. The key frameworks it examines, namely FERC Order 1920's 20-year regional planning scenarios and WECC's extreme-weather sensitivity studies, are precisely where asset-level failure probabilities like those developed in this report could serve as inputs. This report addresses developing some of the asset-level failure information those frameworks need. Together, the two areas close a gap that neither can address alone: the gap between current planning practice and what changing climate conditions will require.

The fragility curves in Section 3 give SCE a probabilistic foundation where only static assumptions currently exist. Each curve converts a specified hazard intensity to a conditional failure probability, which enters a planning model as a concrete parameter rather than an analyst judgment call. The relevant parameters are forced outage rate (FOR) uplifts, line unavailability factors, and substation outage probabilities for use in extreme-weather sensitivity cases consistent with WECC Year-20 study methods [19].

Potential mapping of the three fragility curve models to planning inputs relevant to the companion report [19], is discussed below:

- The wildfire air-gap flashover model (Section 3.1) outputs P(failure | conductor temperature, smoke density); this could feed into a forced outage probability for affected transmission segments under a specified fire-weather scenario for a planning sensitivity case.
- The flooding substation model (Section 3.2) outputs P(DS ≥ k | inundation depth); at DS3 or DS4, this could map to a substation unavailability factor for contingency or power flow studies under a flood-depth scenario.
- The wildfire thermal damage model (Section 3.3) outputs P(failure | conductor temperature), which translates to a line derate or forced outage for conductors with elevated ambient temperature exposure.

All three fragility curve models are provisional; parameters are literature-derived proxies that are not calibrated to specific SCE assets. The appropriate planning use is as a structured starting point that acts as a defensible basis for scenario testing that SCE can refine as internal data becomes available. Additionally, identifying which asset-hazard pairs drive the most planning sensitivity can allow investment in data collection and model development to be prioritized accordingly.

In conclusion, the companion report [19] and this report were written to supplement SCE’s ability to advance climate adaptation from both the process level and the asset level simultaneously.

7. References

[1] A. Serrano-Fontova et al., “A Comprehensive Review and Comparison of the Fragility Curves Used for Resilience Assessments in Power Systems,” IEEE Access, vol. 11, pp. 108050-108067, 2023. DOI: 10.1109/ACCESS.2023.3320579

[2] S. Dian et al., “Integrating Wildfires Propagation Prediction Into Early Warning of Electrical Transmission Line Outages,” IEEE Access, vol. 7, pp. 27586-27603, 2019. DOI: 10.1109/ACCESS.2019.2894141

[3] M. Panteli, C. Pickering, S. Wilkinson, R. Dawson, P. Mancarella, “Power System Resilience to Extreme Weather: Fragility Modeling, Probabilistic Impact Assessment, and Adaptation Measures,” IEEE Trans. Power Systems, vol. 32, no. 5, pp. 3747-3757, 2017. DOI: 10.1109/TPWRS.2016.2641463

[4] G. Fu, S. Wilkinson, R.J. Dawson, H.J. Fowler, C. Kilsby, M. Panteli, P. Mancarella, “Integrated Approach to Assess the Resilience of Future Electricity Infrastructure Networks to Climate Hazards,” IEEE Systems Journal, vol. 12, no. 4, pp. 3169-3180, 2018. DOI: 10.1109/JSYST.2017.2700791

[5] M.R. Jamieson, G. Strbac, K.R.W. Bell, “Quantification and Visualisation of Extreme Wind Effects on Transmission Network Outage Probability and Wind Generation Output,” IET Smart Grid, vol. 3, no. 2, pp. 112-122, 2020. DOI: 10.1049/iet-stg.2019.0145

[6] Y.M. Mohammadi Darestani and A. Shafieezadeh, “Multi-Dimensional Wind Fragility Functions for Wood Utility Poles,” Engineering Structures, vol. 183, pp. 937-948, 2019. DOI: 10.1016/j.engstruct.2019.01.048

[7] A. Shafieezadeh, U. P. Onyewuchi, M. M. Begovic and R. DesRoches, “Age-Dependent Fragility Models of Utility Wood Poles in Power Distribution Networks Against Extreme Wind Hazards,” in IEEE Transactions on Power Delivery, vol. 29, no. 1, pp. 131-139, Feb. 2014, doi: 10.1109/TPWRD.2013.2281265.

[8] K. Murray and K.R.W. Bell, “Wind Related Faults on the GB Transmission Network,” PMAPS 2014, Durham, UK, July 2014.

[9] S. Jazebi, F. de Leon and A. Nelson, “Review of Wildfire Management Techniques – Part I: Causes, Prevention, Detection, Suppression, and Data Analytics,” in IEEE Transactions on Power Delivery, vol. 35, no. 1, pp. 430-439, Feb. 2020, doi: 10.1109/TPWRD.2019.2930055.

[10] G. Karagiannakis, M. Panteli, S. Argyroudis, “Fragility Assessment of Power Grid Infrastructure Towards Climate Resilience and Adaptation,” ESReDA Seminar Proc., Ispra, Italy, Oct. 2023.

[11] “IEEE Guide for Loading Mineral-Oil-Immersed Transformers and Step-Voltage Regulators,” in IEEE Std C57.91-2025 (Revision of IEEE Std C57.91-2011), vol., no., pp. 1-123, 5 March 2026, doi: 10.1109/IEEESTD.2026.11421671.

[12] “IEEE Standard for General Requirements for Liquid-Immersed Distribution, Power, and Regulating Transformers,” in IEEE Std C57.12.00-2021 (Revision of IEEE Std C57.12.00-2015), vol., no., pp. 1-74, 21 Jan. 2022, doi: 10.1109/IEEESTD.2022.9690124.

[13] “IEEE Standard for Test Procedure for Thermal Evaluation of Insulation Systems for Liquid-Immersed Distribution, Power, and Regulating Transformers,” in IEEE Std C57.100-2022 (Revision of IEEE Std C57.100-2011), vol., no., pp. 1-64, 24 March 2023, doi: 10.1109/IEEESTD.2023.10078787.

[14] P. Asaridis and D. Molinari, “A Conceptual Model for the Estimation of Flood Damage to Power Grids,” Advances in Geosciences, vol. 61, pp. 1-21, 2023. DOI: 10.5194/adgeo-61-1-2023

[15] R.C. Rothermel, “A Mathematical Model for Predicting Fire Spread in Wildland Fuels,” USDA Forest Service, Res. Paper INT-115, 1972.

[16] M.A. Finney, “FARSITE: Fire Area Simulator – Model Development and Evaluation,” USDA Forest Service, Res. Paper RMRS-RP-4, 1998.

[17] S. Nematshahi, B. Sohrabi, A. Khodaei, A. Arabnya, and R. Fan, “Wildfire Impact Analysis on Power System Operation: A Framework Leveraging Physics-Based Wildfire Simulation and Dynamic Line Rating,” Electric Power Systems Research, vol. 252, p. 112467, 2026. DOI: 10.1016/j.epsr.2025.112467.

[18] P.M. Fernandes, “Upscaling the Estimation of Surface-Fire Rate of Spread in Maritime Pine (Pinus pinaster Ait.) Forest,” iForest - Biogeosciences and Forestry, vol. 7, no. 2, pp. 123-125, 2014. DOI: 10.3832/ifor0992-007

[19] University of Michigan SEAS Capstone Team, “Integrating Future Climate Data into Transmission Planning in California,” Report to Southern California Edison, February 2026.

[20] Southern California Edison / Edison International, “Adapting for Tomorrow: Powering a Resilient Future,” Climate Adaptation Vulnerability Assessment, filed with the California Public Utilities Commission, May 13, 2022. Available at: https://www.sce.com/about-us/environment/climate-adaptation.

[21] F. J. Doblas-Reyes et al., “Chapter 12: Climate Change Information for Regional Impact and for Risk Assessment,” in Climate Change 2021: The Physical Science Basis. Contribution of Working Group I to the Sixth Assessment Report of the Intergovernmental Panel on Climate Change, V. Masson-Delmotte et al., Eds. Cambridge University Press, 2021, pp. 1767-1926. DOI: 10.1017/9781009157896.014

[22] National Centers for Environmental Information (NCEI), “U.S. Climate Normals (1991-2020),” National Oceanic and Atmospheric Administration. Available: https://www.ncei.noaa.gov/products/land-based-station/us-climate-normals

[23] Federal Emergency Management Agency (FEMA), “Hazus Flood Model Technical Manual, Hazus 7.0,” FEMA, June 2025. Available: https://www.fema.gov/sites/default/files/documents/fema_rsl_hazus-7-fltm_06272025_0.pdf

[24] M. Nazemi, P. Dehghanian, Y. Darestani, and J. Su, “Parameterized Wildfire Fragility Functions for Overhead Power Line Conductors,” IEEE Trans. Power Systems, vol. 39, no. 2, pp. 2517-2527, 2024. DOI: 10.1109/TPWRS.2023.3298769